Supplementary information

Exceptionally potent human monoclonal antibodies are effective for prophylaxis and therapy of tetanus in mice

Pirazzini et al.

Figure S1: Representative western blotting of TeNT polypeptide chains, domains and sub-domains recognition by the repertoire of human monoclonal antibodies produced by immortalized clonal B memory cells

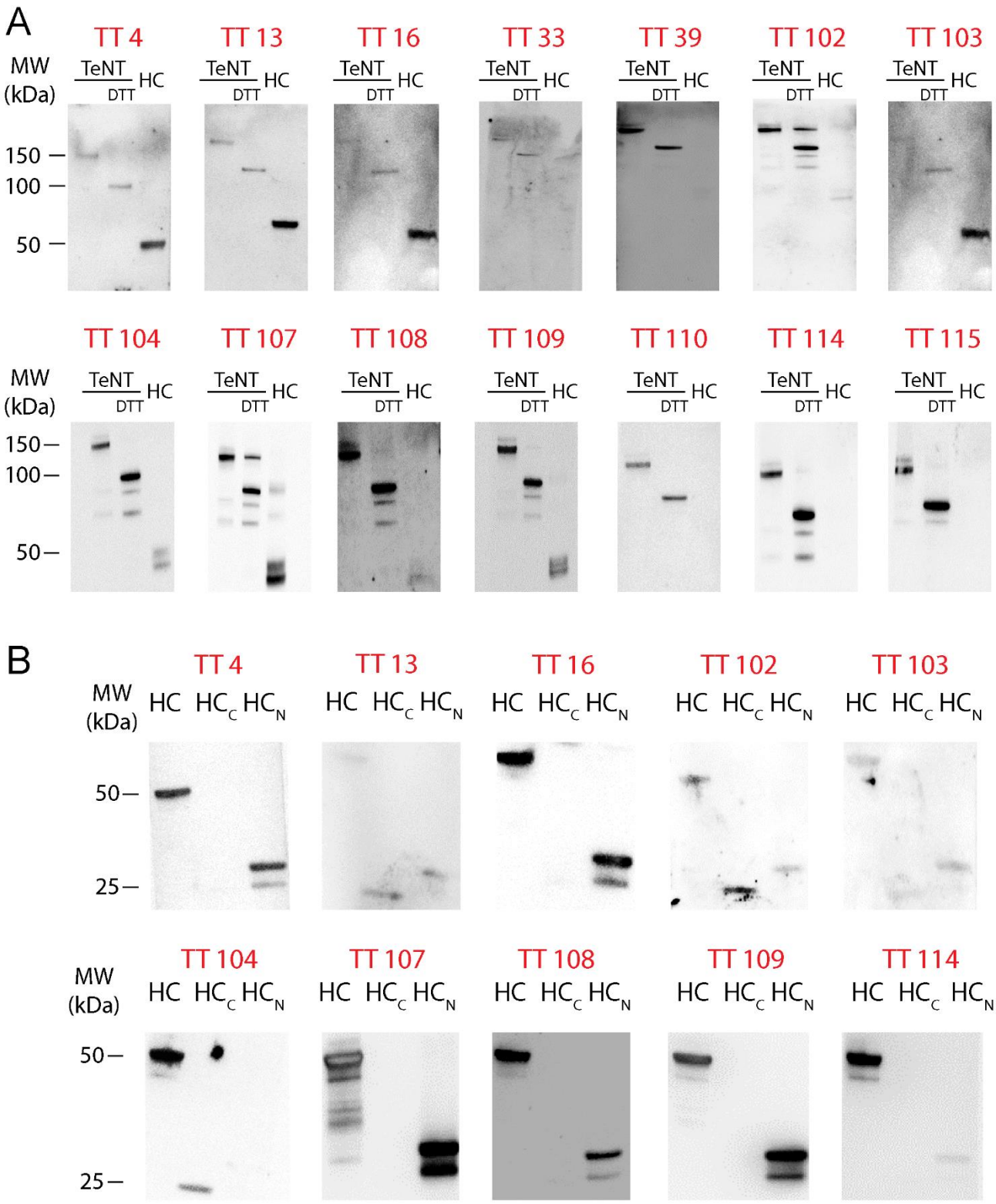

Figure S2: Structure of an immunoglobulin G showing its different domains and the site in the heavy chain where the stop codon was inserted to generate the Fabs. Below are the sequence for TT104 and TT110 Fabs.

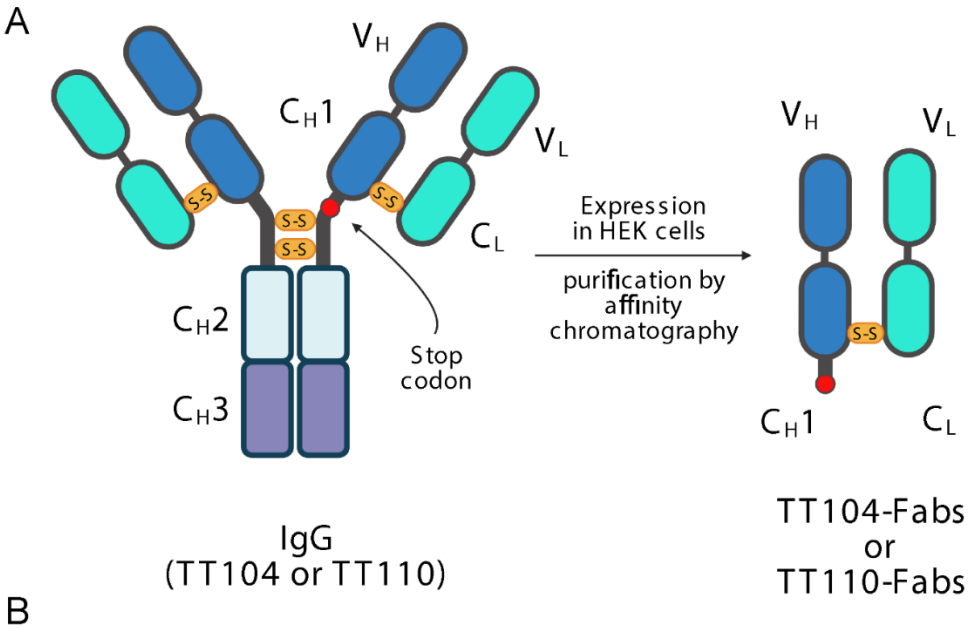

B

vH_104

QLQLQESGPGLVRPSETLSLTCSVSDDSMGSSTYYWAWIRQPPGKGLEWIGNVYYNGVTYYNSSLESRLTLSI
DPSKNQFSLILSSVTAADTAVYYCARQADNWFDPWGQGTLVTVSSASTKGPSVFPLAPSSKSTSGGTAALGCL
VKDYFPEPVTVSWNSGALTSGVHTFPAVLQSSGLYSLSSVVTVPSSSLGTQTYICNVNHKPSNTKVDKRVEPK
SCE

vL_104

IMMTQSPATLSVSPGERATLSCRASQSVGSDLAWYQQKPGQAPRLLIYGASYRATGIPARFSGGGSGTEFTLT
ISSMQSEDFAVYYCQQYYNWPPYTFGQGTKVEIKRTVAAPSVFIFPPSDEQLKSGTASVVCLLNNFYPREAKV
QWKVDNALQSGNSQESVTEQDSKDSTYSLSSTLTLSKADYEKHKVYACEVTHQGLSSPVTKSFNRGEC

vH_110

QVQLMQSGAEVQKPGASVKVSCQASGFTLNNYYIHWLRQAPGQGFEWMGIFNPSSGTRTYAQKFQGRISMTAD
ASTTTLYMELSGLTSEDAGVYFCARIGGSTYGRLMTYYFDHWGQGTVVAVSSASTKGPSVFPLAPSSKSTSGG
TAALGCLVKDYFPEPVTVSWNSGALTSGVHTFPAVLQSSGLYSLSSVVTVPSSSLGTQTYICNVNHKPSNTKV
DKRVEPKSCE

vL_110

VLTQGPVTLSVSPGGRGTLSCRASRSISTTLAWYQQKPGQAPRLLIYGASTRATGIPARFTGSGSGTEFTLTI
SSLQSEDFAVYYCQQYNDWPVTFGQGTQVEVKRTVAAPSVFIFPPSDEQLKSGTASVVCLLNNFYPREAKVQW
KVDNALQSGNSQESVTEQDSKDSTYSLSSTLTLSKADYEKHKVYACEVTHQGLSSPVTKSFNRGEC

Figure S3: TeNT binding of TT104-Fab and TT110-Fab assayed by surface plasmon resonance. SPR analysis of the interaction between TeNT and TT104-Fab (A) and TT110-Fab (B). TeNT was immobilized on a TRIS-Ni-NTA sensor chip. Sensograms show the binding of incremental concentrations of Fabs on the sensor chip. The binding data were analyzed with a one site binding model.

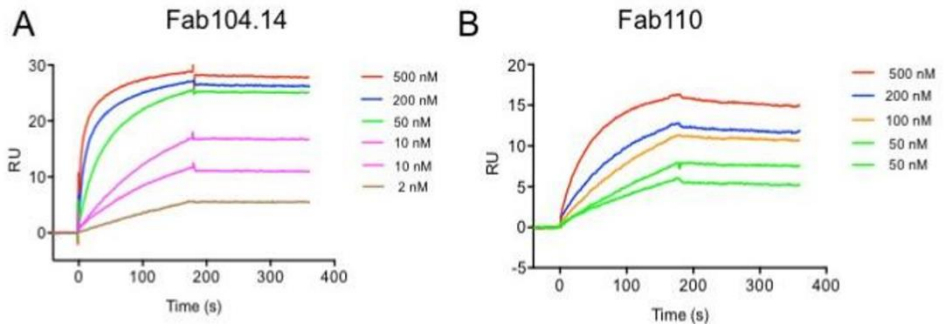

	K_a (1/Ms)	K_d (1/s)	K_D (M)
TeNT-TT104-Fab	$4{,}5*10^{-5}$	$3{,}0*10^{-6}$	$6{,}7*10^{-12}$
TeNT-TT110-Fab	$6{,}3*10^{-4}$	$2{,}5*10^{-4}$	$3{,}0*10^{-9}$

Figure S4: Size exclusion chromatography (SEC) and native polyacrylamide electrophoresis analysis of TeNT immunocomplexes. TeNT (violet trace), TeNT and TT104-Fab (red trace), TeNT and TT110-Fab (grey trace) or TeNT and the two Fabs together (ternary immunocomplex, blue trace). SEC analysis was performed with a Superdex 200 10/300 column (GE Healthcare) and respective peaks were analyzed on native gels.

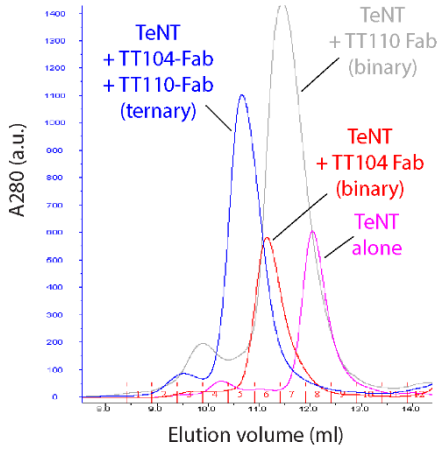

Figure S5: Cryo-EM image processing. A) from top to bottom: representative cryo-EM micrograph from untilted (left) and 30° tilted (right) data acquisition; selection of typical 2D class averages used for 3D reconstruction; results of the 3D global refinement; initial body used for multibody refinement; result of the multibody refinement and their associated FSC curves. B) contributions of all eigenvectors to the variance. The structure in fig. 3 C-D corresponds to the extreme of the first eigenvector. C) Histogram of the amplitudes along the first eigenvector shows a unimodal distribution.

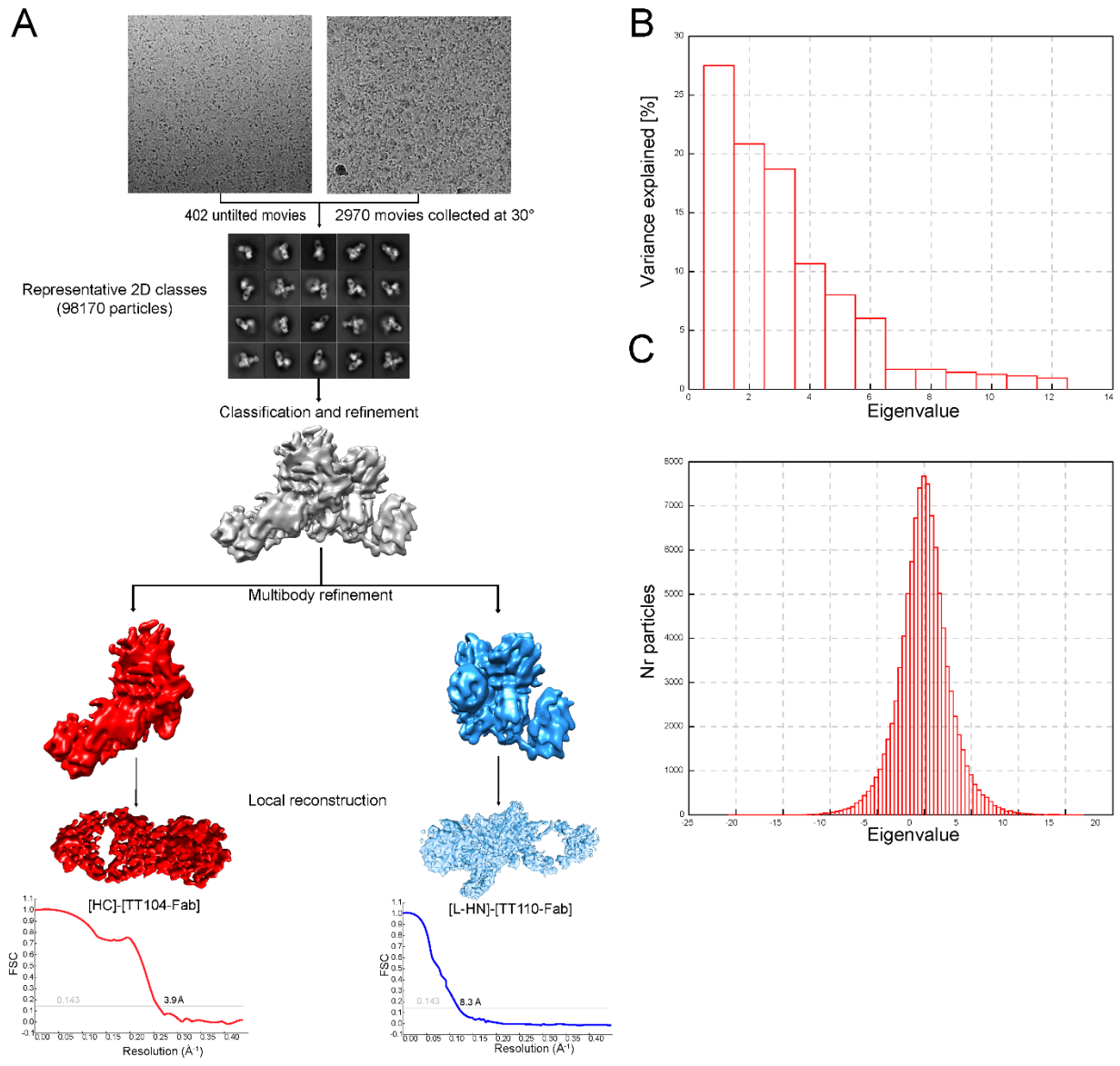

Figure S6: Representation of TT104-Fab bound to TeNT HC also in complex with nidogen. Nidogen binding is represented as previously modelled before (1). Spheres indicate the clashes predicted to occur between nidogen and TT104-Fab.

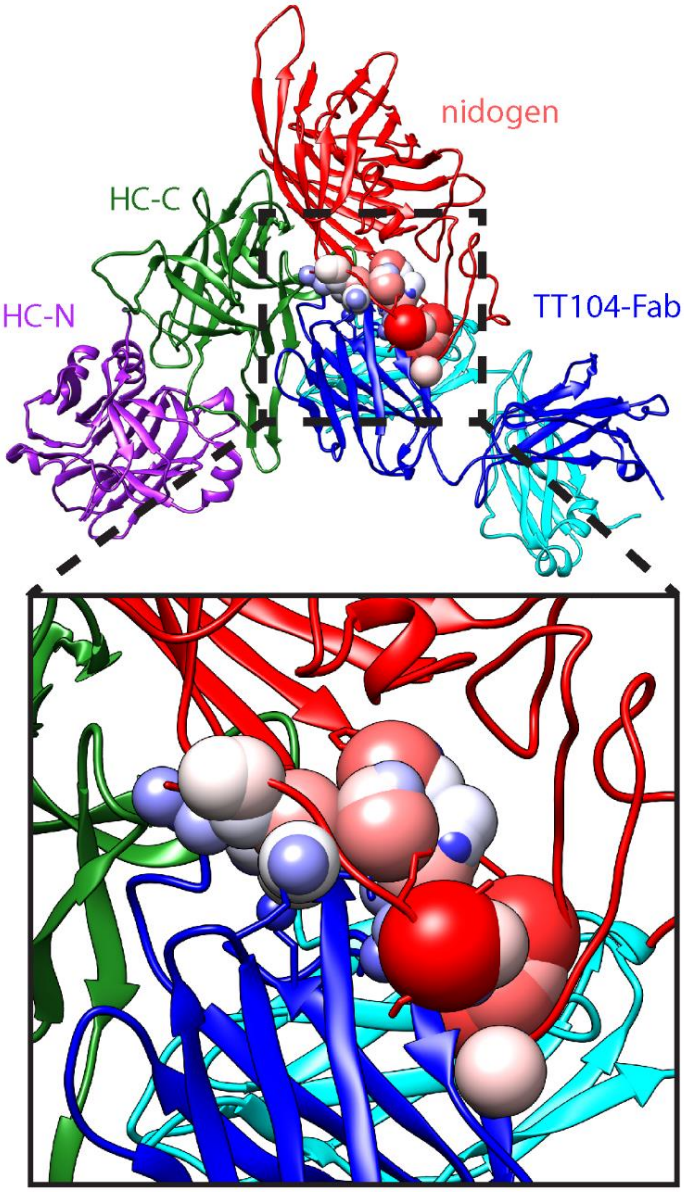

Figure S7. The BoNT switch is also present in TeNT. Representation of the HN domains of BoNT/A (left) and TeNT (right), where the BoNT switch is highlighted in red. Both structures display a very similar arrangement of this structural motif that was recently predicted to be the first part of the BoNT molecule that inserts into the membrane during the translocation process (Lam et al., 2018).

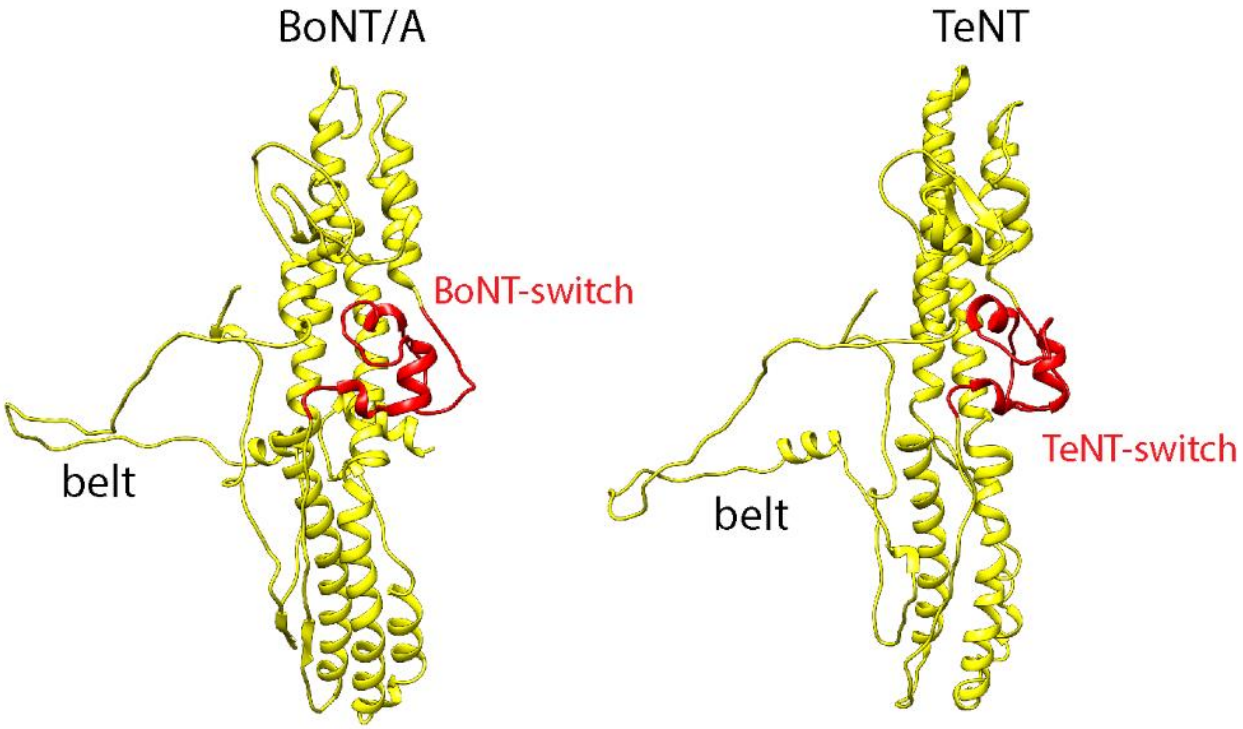

Figure S8: Cartoon representation of TT110-Fab bound to TeNT HN highlighting carboxylate residues possibly involved in the low pH induced structural change of BoNT and TeNT structure. The top panel shows the large area of the TeNT epitope recognized by the Fab derivative of the humAb TT110. The lower panel shows a close up view of the Fab interaction with the central helix of the "TeNT-switch", which corresponds to the α_B helix of the BoNT-switch in BoNT/A (2). The helices of the HN domain of TeNT, marked in red, correspond to the helices in α_A and α_C of the BoNT-switch, respectively. In orange it is highlighted another helix within the HN domain of TeNT which is part of the epitope recognized by the TT110-Fab. In green are the carboxylate residues suggested by the present study to play an essential role in the HN structural change caused by acidification inside synaptic vesicles.

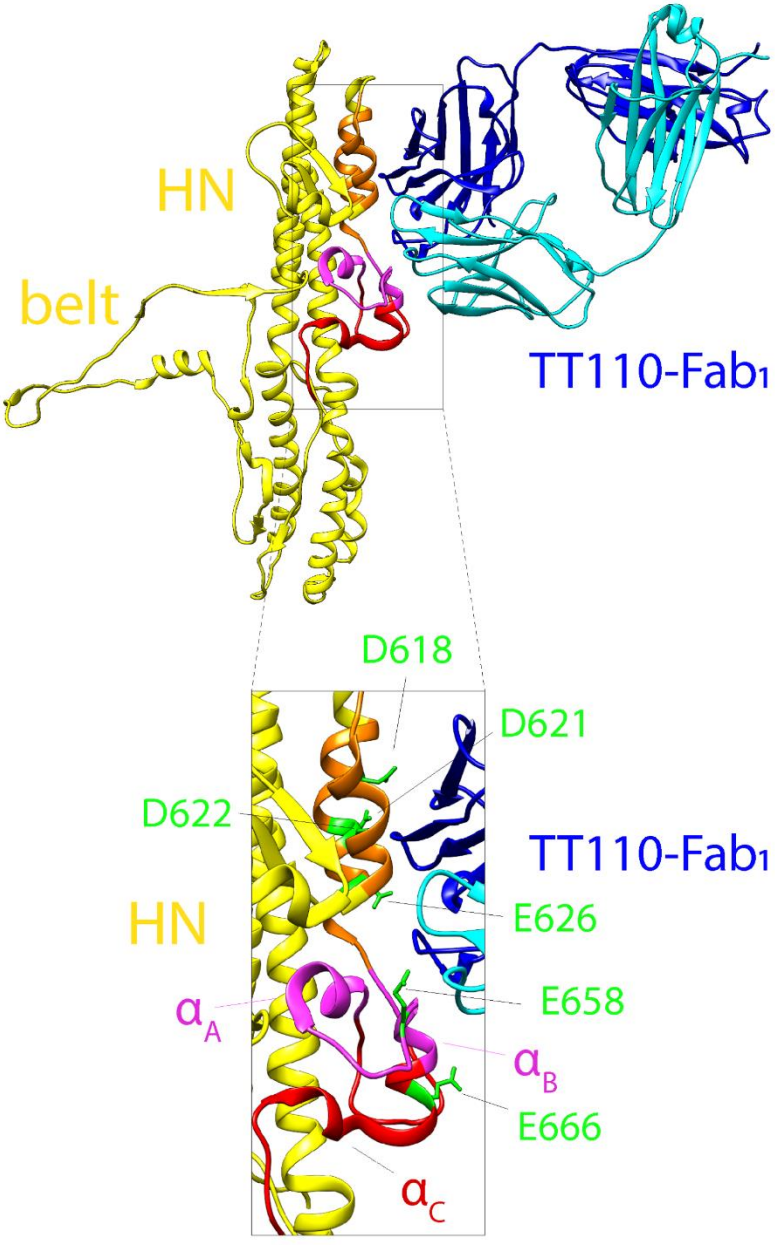

Supplementary Table 1. Atomic details of TeNT-TT104-Fab interaction. H-bond and salt bridge interactions and between the HC domain of TeNT and TT104-Fab, as detected by server PISA (https://www.ebi.ac.uk/pdbe/pisa/).

	HC	Chain B	Chain A
H-bond	Lys1143 O	Ser32 OG	
H-bond	Gln1141 NE2	Thr33 O	
H-bond	Asn1153 OD1	Asn103 ND2	
H-bond	Asn1153 ND2	Asn103 OD1	
H-bond	Tyr1202 OH	Ser31 O	
H-bond	Tyr1202 OH	Ser32 O	
H-bond	Tyr1150 OH	Asp102 OD1	
H-bond	Asn1153 ND2		Tyr318 OH
H-bond	Ser1156 N		Asn314 O
Salt Bridge	Arg1281	Asp102	

Supplementary Table 2. Model quality.

	HC- TT104-Fab	LC-HN-TT110-Fab
Residues/atoms	870 / 6830	
RMSD bond length (Å) Angles (°)	 0.009 1.16	
MolProbity score	3.43	
Ramachandran plot (%) Favored Allowed Outliers	 70.65 29.23 0.12	
CC (mask/box)	0.78 / 0.79	

Legends of Supplemental videos

Supplemental Video 1: Repositioning of the reconstructed bodies' densities of the TeNT domains along the first eigenvector.

Supplemental Video 2: Repositioning of the reconstructed bodies' densities of the TeNT domains along the second eigenvector.

Supplemental Video 3: Repositioning of the reconstructed bodies' densities of the TeNT domains along the third eigenvector.

Supplemental Methods

Reagents

All chemicals used were from Sigma Aldrich. TeNT was previously isolated from culture filtrates of *C. tetani* strain Y-IV-3 (WS 15), frozen in liquid nitrogen and stored at -80°C in 10 mM HEPES-NaOH, 50 mM sodium chloride, pH 7.2.

TeNT HC (residues 875-1,315) was N-terminally fused with glutathione *S*-transferase (GST) and expressed in *E. coli* as previously described (3). Where indicated, TeNT HC was labeled with AlexaFluor555-maleimide following manufacturer's instructions and dialyzed against 10 mM HEPES-NaOH, 150 mM NaCl, pH 7.4. TeNT HC-N (residues 856-1,110) and HC-C (residues 1,111-1,315) were expressed in *E. coli* as GST fusion proteins and purified as previously described (3). HC BoNT/A1 (residues 876-1296) was N-terminally fused with CpV (Circularly permutated Venus), cloned into a pET28a His-tag vector (Novagen) and expressed in *E. coli*. Purification was performed with a prepacked HisTrap Ni column (GE Healthcare) as previously described (4). Protein concentration was determined by absorption spectroscopy and purity by SDS-PAGE.

TeNT-Fabs complexes formation and purification

TeNT and the two Fabs were incubated at 4°C overnight under stirring. The complex formed was purified from unbound Fabs by gel filtration (Superdex 200 10/300**,** GE) and analyzed by a Native-PAGE analysis in buffer 10 mM Tris, 150 mM NaCl, pH 7.4 and visualized in 4-16% native-PAGE gel (ThermoFischer Scientific). The fractions containing the ternary complex were collected and concentrated until a final volume of 500 µl, and subsequently loaded on a gel filtration column. The first peak corresponds to complex TeNT-Fabs (250 kDa) and the second peak at lower molecular weight corresponds to the unbound Fabs (104 and 110). The ternary complex was purified by gel filtration. Native-PAGE gel confirmed that in the peak are present both TeNT, TT104-Fab and TT110-Fab and that the ternary immunocomplex eluted as a homogeneous physical species. At variance, the second peak contained the unbound Fabs and eluted at the same elution volume (data not shown). The peak corresponding to [TeNT]-[TT104-Fab]-[TT110-Fab] was isolated and concentrated to 1 mg/ml.

Surface Plasma Resonance (SPR) analysis

For the SPR analysis, a BIAcore™ T100 system (GE Healthcare) was used. TeNT was covalently coupled to a CM5 (series S) sensor chip (carboxymethylated dextran surface) by amine-coupling chemistry to a final density of 1000 resonance units, as described (66). Binding analysis was carried out in a running buffer consisting of 10 mM Hepes-NaOH, pH 7.6, 150 mM NaCl, 2 mM $MgCl_2$, using a flow rate of 30 μl/min. Each sensogram was corrected for the response obtained in the control flow cell and normalized to baseline. After each injection, the surface was regenerated by a double injection of 1M NaCl for 1 min to restore the base line to the initial resonance unit value. For kinetic experiments, a BIAcore™ method program was used that included a series of three start-up injections (running buffer), zero control (running buffer), and five different dilutions in running buffer of the TT104-Fab (500, 200, 50, 10, 2 nM) and four for TT110-Fab (500, 200,100, 50 nM). The contact time was 180 s followed by a 200 s dissociation phase. Kinetic data were analyzed with the 2.0.3 BIAevaluation software (GE Healthcare). The curves (both association and dissociation phases) were fitted with the classical Langmuir 1:1 model; the quality of the fits was assessed by visual inspection of the fitted data and their residuals, and by chi-squared values. Two independent experiments in triplicates were performed.

Model building and refinement

The two maps were visualized and treated separately because of their different resolutions. The crystal structure of TeNT (5) (PDB ID 5n0b) was divided in two files, one including only the HC domain, the domain HN and domain L. The homology models of the structure of the two Fabs were generated via SwissModel (6) using the PDB ID 5dk3 e 1hzh as a template. All models were fitted as rigid bodies using Chimera (7). The HC and TT104-Fab models were fitted in the appropriate map. For the Fab, the two positions rotated by 180° around the molecular pseudo-symmetry axis were tested, and the positions that gave significantly better interactions with the toxin were used. The model was improved by iterative cycles of Phenix real space refinement (8) and visualized with Coot (9). Model refinement was carried out using geometry restraints, including secondary structure, rotamer and Ramachandran plot restraints. Finally, the map was sharpened according with the PDB model's B-factor using Phenix. The final statistics on the refined models are reported in Supplementary Table 2. The HN and L chain domains and TT110-Fab were fitted in the second map; owing to the remaining preferential orientation symptom, the quality of the map allows only to perform a rigid body fitting of the already existing structures (5).

Cell cultures of cerebellar granule neurons

Primary cultures of rat cerebellar granule neurons (CGNs) were prepared from 4- to 6-day-old rats. Cerebella were isolated, mechanically disrupted and trypsinized in the presence of DNase I. Cells were then collected and plated into 24-well plates pre-coated with poly-L-lysine (50 μg/ml) at a cell density of $4x10^5$ cells per well or onto 13 mm round glasses at a cell density of $3x10^5$ cells per well. Cultures were maintained at 37˚C, 5% CO2, 95% humidity in BME (Basal Medium Eagle) supplemented with 10% fetal bovine serum, 25 mM KCl, 2 mM glutamine and 50 μg/ml gentamicin (here after indicated as complete culture medium). To arrest growth of non-neuronal cells, cytosine

arabinoside (10 µM) was added to the complete culture medium 18–24 h after plating. Neurons were used after 6 days *in vitro* and to a maximum of 8 days *in vitro*.

Supplemental References

1. Bercsenyi K, Schmieg N, Bryson JB, Wallace M, Caccin P, Golding M, et al. Nidogens are therapeutic targets for the prevention of tetanus. *Science.* 2014;346(6213):1118-23.

2. Lam KH, Guo Z, Krez N, Matsui T, Perry K, Weisemann J, et al. A viral-fusion-peptide-like molecular switch drives membrane insertion of botulinum neurotoxin A1. *Nat Comm.* 2018;9(1):5367.

3. Herreros J, Lalli G, Montecucco C, and Schiavo G. Tetanus toxin fragment C binds to a protein present in neuronal cell lines and motoneurons. *J Neurochem.* 2000;74(5):1941-50.

4. Azarnia Tehran D, Zanetti G, Leka O, Lista F, Fillo S, Binz T, et al. A Novel Inhibitor Prevents the Peripheral Neuroparalysis of Botulinum Neurotoxins. *Sci Rep.* 2015;5:17513.

5. Masuyer G, Conrad J, and Stenmark P. The structure of the tetanus toxin reveals pH-mediated domain dynamics. *EMBO rep.* 2017;18(8):1306-17.

6. Waterhouse A, Bertoni M, Bienert S, Studer G, Tauriello G, Gumienny R, et al. SWISS-MODEL: homology modelling of protein structures and complexes. *Nucleic Acid Res.* 2018;46(W1):W296-W303.

7. Pettersen EF, Goddard TD, Huang CC, Couch GS, Greenblatt DM, Meng EC, et al. UCSF Chimera--a visualization system for exploratory research and analysis. *J Comput Chem.* 2004;25(13):1605-12.

8. Afonine PV, Poon BK, Read RJ, Sobolev OV, Terwilliger TC, Urzhumtsev A, et al. Real-space refinement in PHENIX for cryo-EM and crystallography. *Acta Crystallogr D Struct Biol.* 2018;74(Pt 6):531-44.

9. Emsley P, and Cowtan K. Coot: model-building tools for molecular graphics. *Acta Crystallogr D Biol Crystallogr.* 2004;60(Pt 12 Pt 1):2126-32.